DOE SC-NE Workshop on Advanced Computational Materials Science for Fusion and Fission Reactors

March 31-April 2, 2004

Washington, DC

Long-Term Radiation Effects in Fission & Fusion Reactors

Bill Wolfer, Alison Kubota, Michael Surh, Taira Okita, Jess Sturgeon, Frank Garner, Kazunori Morishita

Theory and computation address many scientific issues:
Secondary Defect Cluster Formation
Energies of Helium-Vacancy Clusters
Helium Diffusion
Bubble Nucleation and Growth
Effects of Bubbles on Mechanical Properties
Void Swelling: Incubation versus Steady State Rate
Effects of Impurities, Temperature, Dose Rate, and Dislocations on the Incubation Dose
Crystal Structure and Propensity for Void Swelling

Radiation damage processes span vast length and time-scales

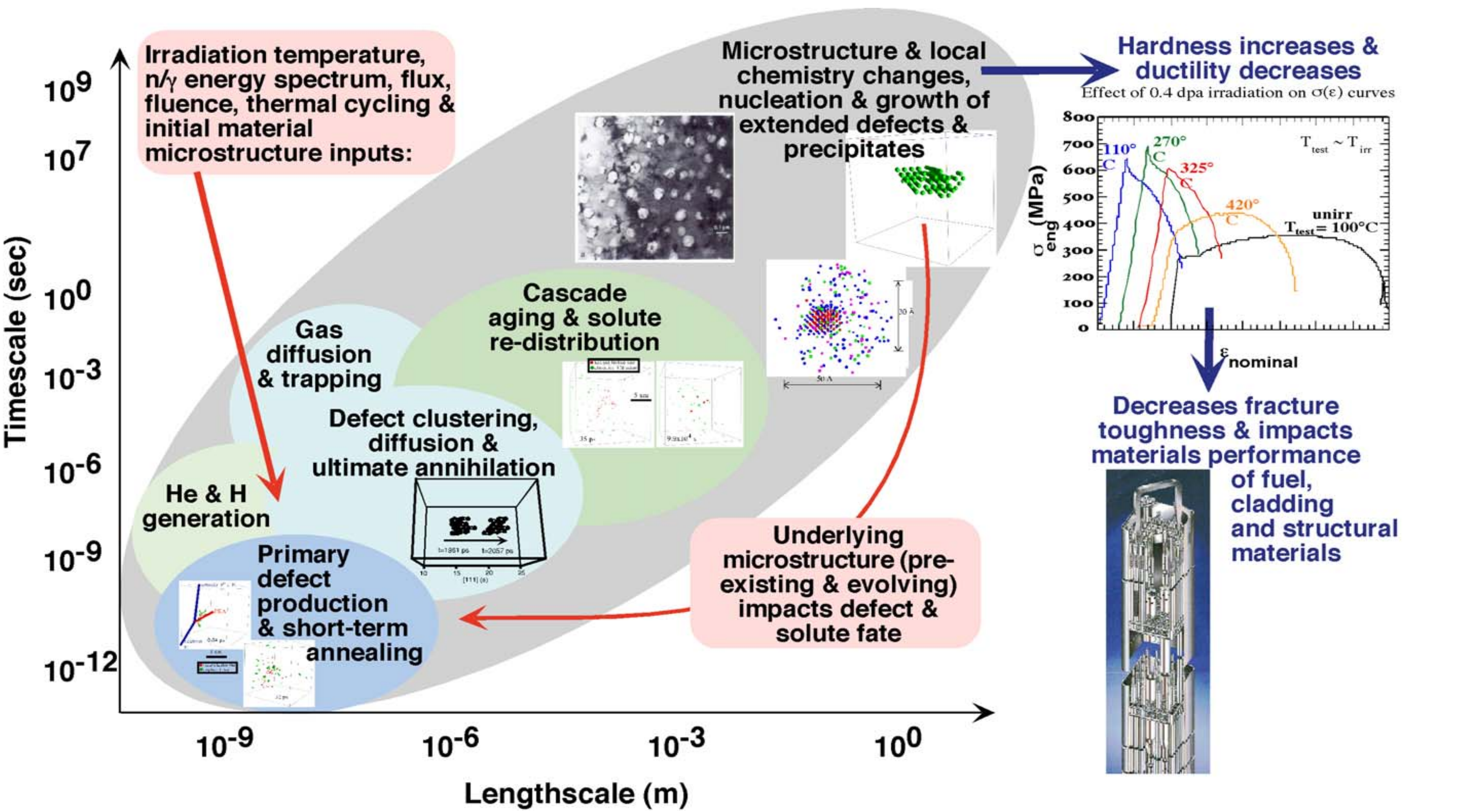

First-principle and atomistic simulations continue to play ever greater roles in radiation effects and in materials science

- From Marlowe, TRIM, to MDCASK, molecular dynamics simulations have played the key role to understand and model primary defect production in collision cascades and surface erosion by sputtering.
- kMC are essential to investigate defect clustering in cascade and to determine the fraction of freely-migrating defects.
- First-principle electronic structure methods are now used to determine fundamental properties of point defects and diffusion of alloying elements in steels.
- Atomistic simulations have revealed the high mobility of interstitial clusters and small dislocation loops.
- Atomistic simulations are useful to determine energies of defect clusters.
- Atomistic simulations of defect-dislocation interactions enabled us to understand radiation embrittlement of reactor vessels.

The domain where long-term effects arise is between Stage III and V

- Nearly all primary defects and transmutants are mobile.
- Most alloying elements are mobile and can reconfigure into new precipitates and/or segregation gradients.
- Secondary defects are prismatic dislocation loops, SFT, voids, bubbles, and a dislocation structure of dominant edge character.
- Microstructure of secondary defects leads to changes in mechanical properties (elastic, plastic, fracture, creep) and density or dimensional changes.
- Domain of full mobility is determined by temperature and dose rate.
- Helium and hydrogen effects become dominant near and above Stage V.
- A most important ingredient in secondary microstructure evolution is biased diffusion.
- The evolutions of secondary vacancy- and interstitial-type defects are coupled, and the coupling mechanisms also evolve.

MD Simulations of 20 keV Recoils in Nanocrystalline Copper: Interaction of Cascades with Existing Grain Boundaries and Extended Defects

By Alison Kubota and Maria Cartula

5 psec after Cascade, (partial cut representation)
Cascade debris coalesces into SFTs and partial dislocations

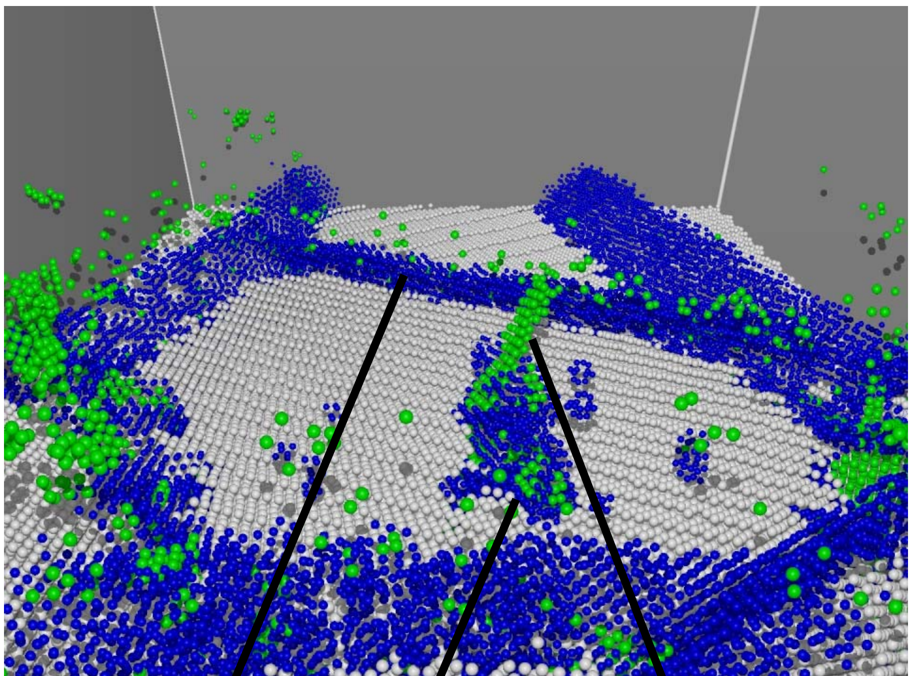

Stacking Fault Tetrahedra (SFT)

Dislocation

Grain Boundary

200 psec after Cascade (partial cut representation)
Partial dislocations and SFTs collapse into stable stacking faults

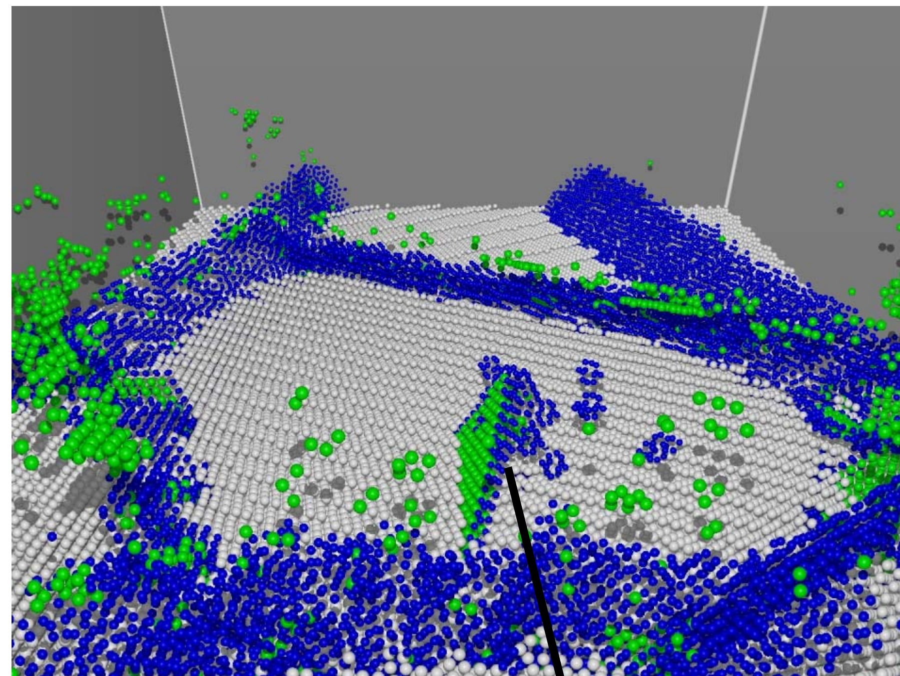

Stacking Fault (SFT)

20 nm x 20 nm x 20 nm Cu supercell containing over 1 million atoms
10 nm average size grain boundaries
Partial Dislocation and Stacking fault extend fully to the grain boundary

White = locally fcc structured atoms
Green = locally hcp structured atoms
Blue = locally disordered atoms

Binding Energies depend on the He/Vacancy Ratio

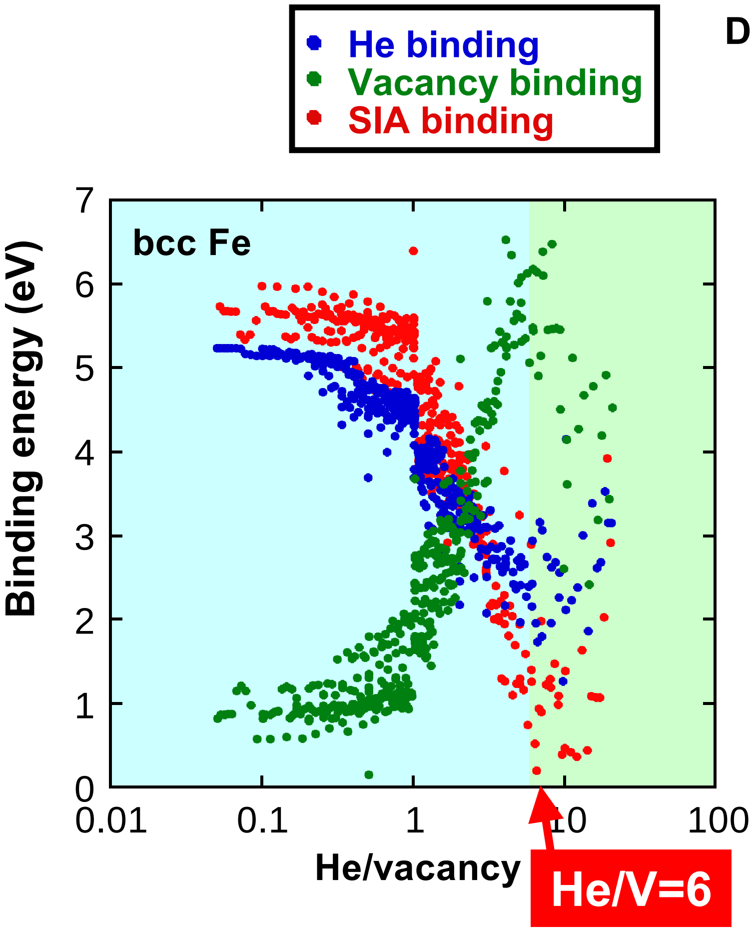

Binding energies of interstitial He, vacancy and SIA to a He_nV_m cluster as a function of helium-to-vacancy ratio (n/m).

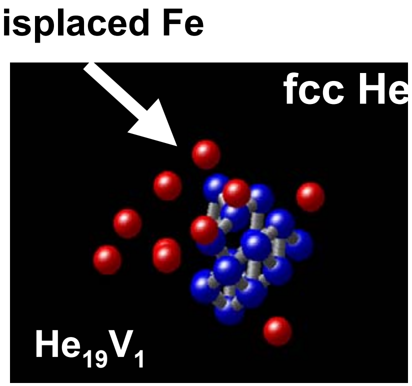

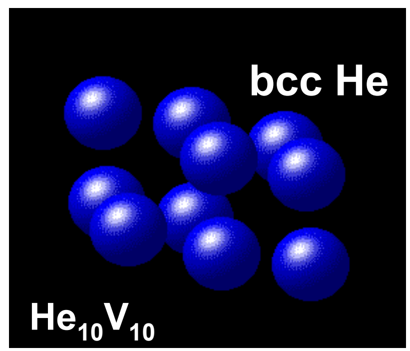

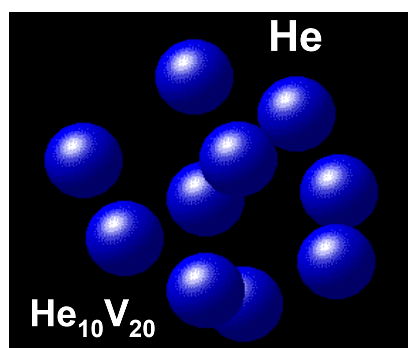

He/vacancy > 6

- Close-packed configuration of He
- A cluster push Fe lattice atom off from its normal site.
- By spontaneous creation of SIA, a cluster can obtain additional vacancy, resulting in 'effective' decrease in He/V ratio. It is reflected by a change in the trends of binding energy curves at He/V=6.

He/vacancy = 1

- bcc structure of He (coherent with bcc Fe matrix)

He/vacancy < 0.5

- Not crystalline

Prof. Morishita
Kyoto University

Diffusion of He, SIA and vacancy in bcc (& fcc) Fe by MD simulation

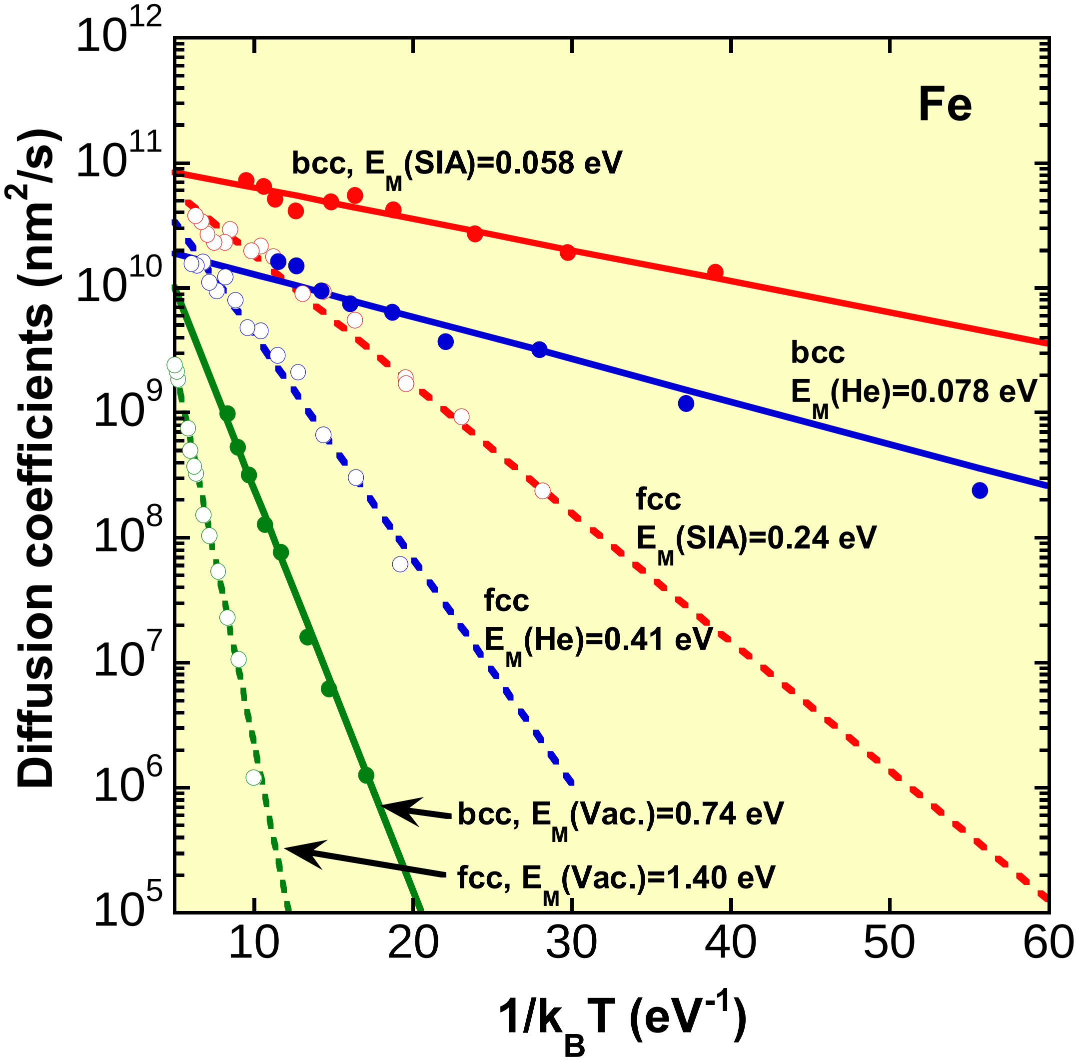

Prof. Morishita

Diffusion coefficients are obtained from migration distances of the defect during 1-100 nsec as a function of temperature.

Diffusion coefficient

$$D = \frac{\left\langle \left\{ \vec{r}(t+\Delta t) - \vec{r}(t) \right\}^2 \right\rangle}{6\Delta t}$$

$\vec{r}(t)$ **:position vector of defects**

Helium bubbles form when there are no voids to be found

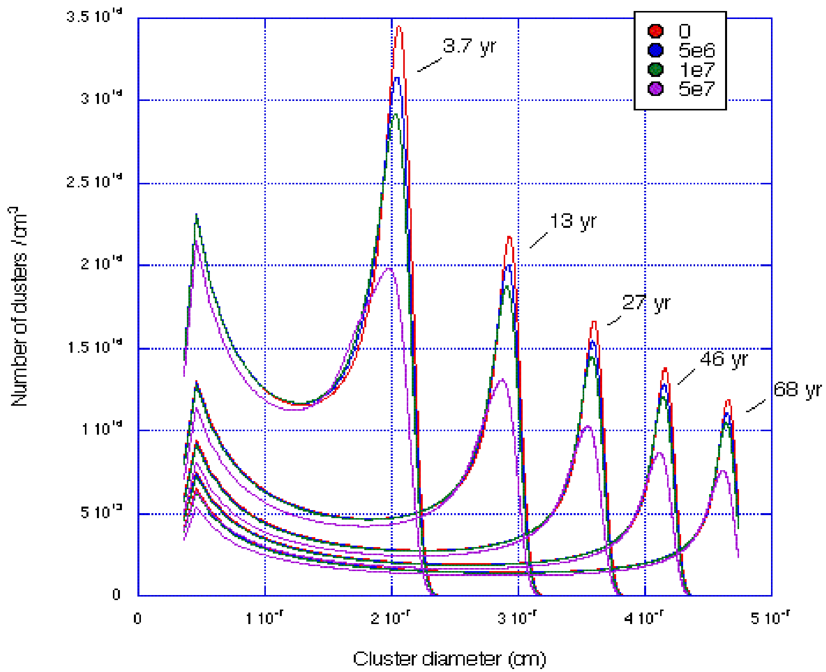

It depends on the helium generation rate and the void sink strength.
For 10^(- 5) appm/s,
no bubbles form when void sink strength exceeds
10^(8) cm^(- 2)

Mainly voids
Void & Helium Bubbles
Helium bubbles only

He/dpa ratios, appm/dpa

FFTF 304 SS	EBR-II 304 SS	HIFR PTP 304 SS	HIFR PTP Ni	Fusion Steels	PWR Baffle Bolt	BWR Grid Plate	Pu	PdT
0.1-1	0.2-0.3	60	600	14	14-25	72	400	infinite

Hydrogen storage in HFIR-irradiated USPCA containing $4x10^{17}$ cm^{-3} "helium-filled cavities" at 34 dpa at 400ºC

Tanaka et al., 1988

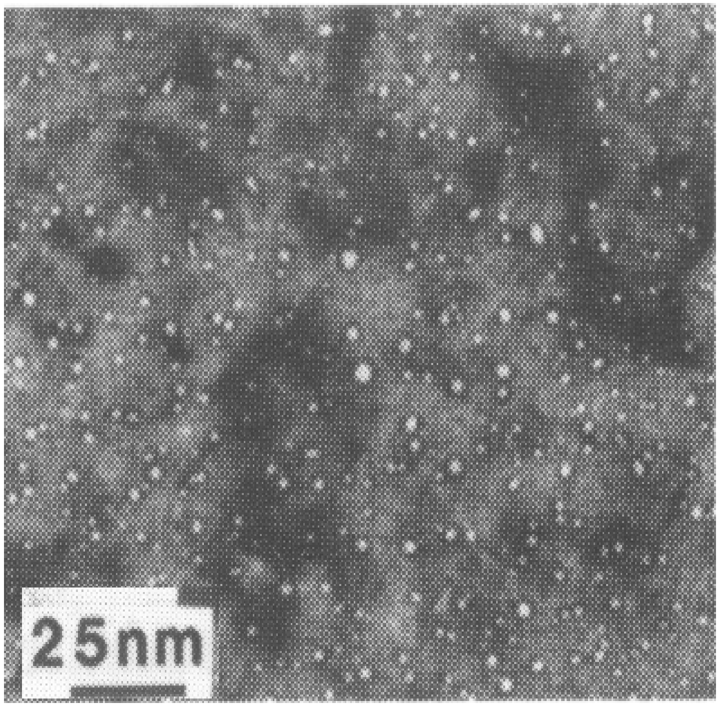

JP-12 experiment

Specimens were irradiated in an aluminum gas-gapped assembly,filled with helium and **never touching water.**

After 13 years of storage in a dry canister, the gas contents of two specimens were measured.

2979 and 3012 appm He

3864 and 3790 appm H

High pressure equations of state for hydrogen and helium must be used

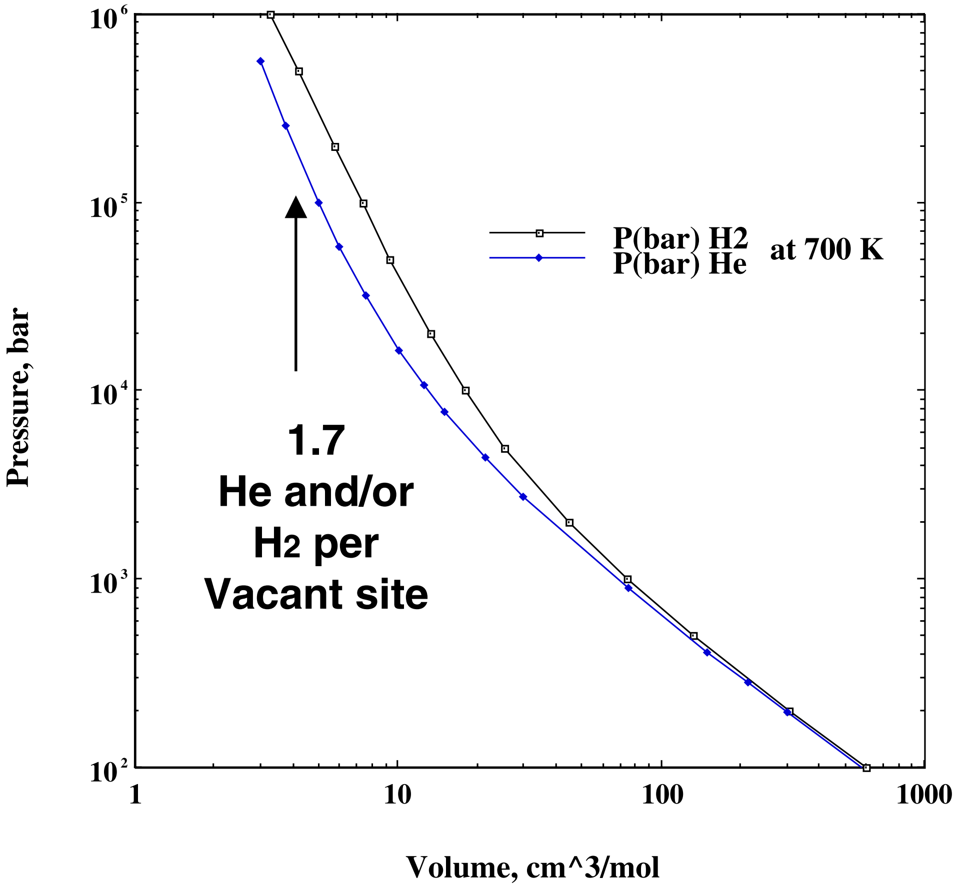

Assuming 400ºC and microstructure observed in the HFIR case, there are 1.7 gas atoms or molecules stored per vacant atomic site.

Gas pressure in bubbles is calculated to be ~20 GPa, approaching stress level required for growth by dislocation loop punching.

Sievert's law would require a hydrogen concentration of 1.8%

Displacement damage can result in non-thermal release of helium from bubbles

By Alison Kubota

20000 eV
3500 eV
630 eV
112 eV
20 eV

This 20-keV Cu recoil in Cu near a 1-nm diameter He bubble produced several ejected He.

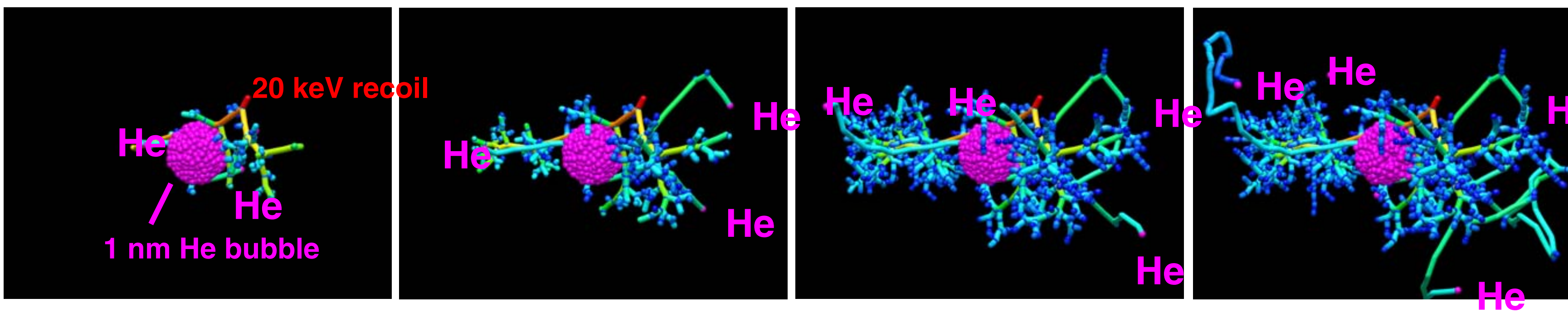

0.045 ps: 20 keV early casade track producing 2 He energetic recoils.

0.077 ps: 20 keV early casade track, 3rd He recoil produced.

0.14 ps: Full cascade bloom, 4th He recoil produced.

0.37 ps: Larger overlap between cascade bloom and bubble to produce secondary He.

Many simulations are needed to obtain statistically meaningful results

Impure alloys appear to have long incubation doses
High-purity alloys much shorter ones

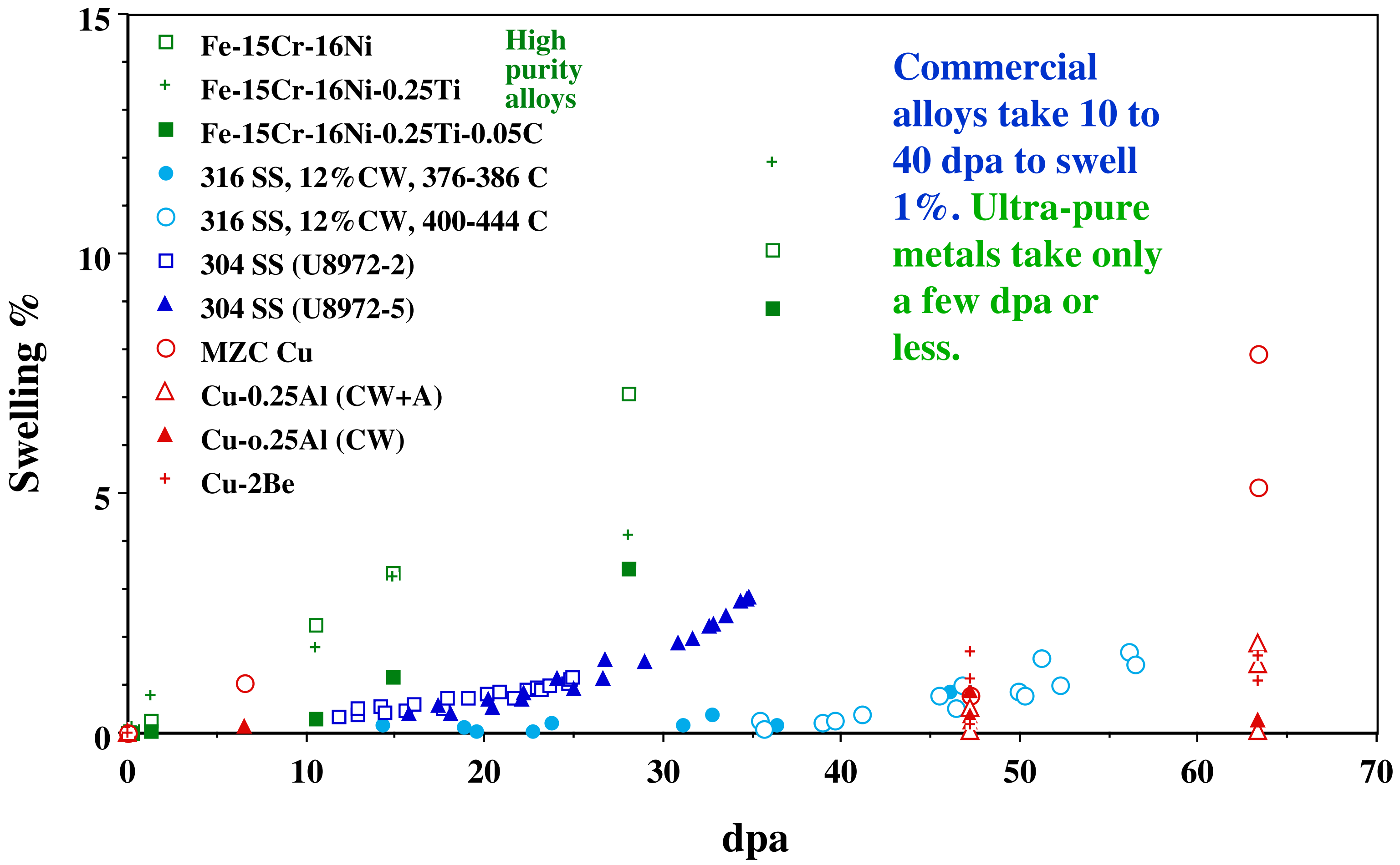

A crucial question is the onset of void swelling and its extrapolation to different damage rates

Okita et al.

Pure 69% Fe, 15% Cr, 16% Ni
FFTF MOTA, 387-444 C

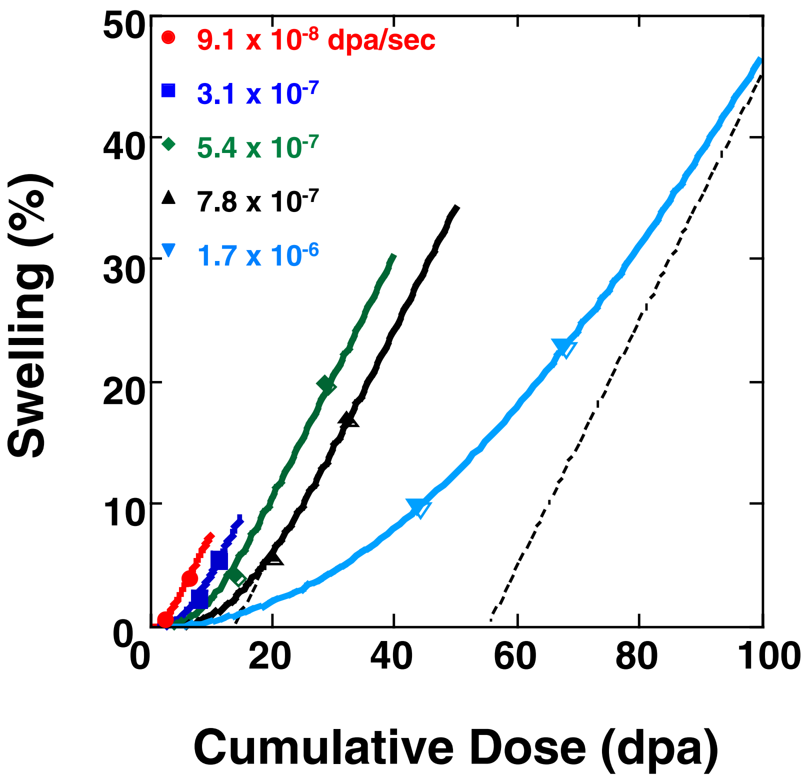

Garner et al., PNNL

SS 304, EBR-II Data / PNNL-Mitsubishi Study

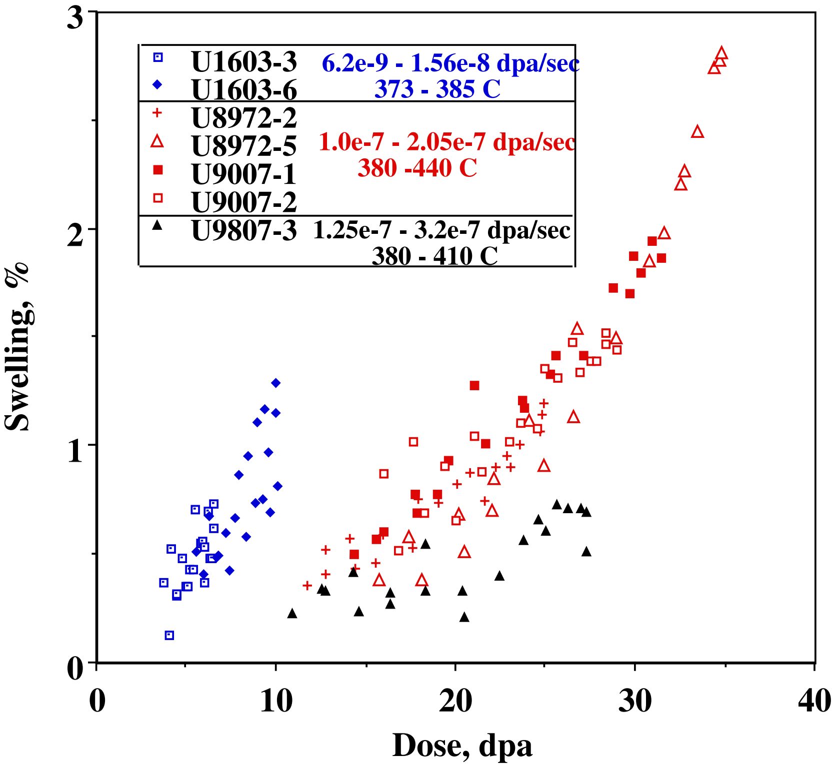

Void Nucleation and Growth can now be followed computationally from 0.001 to 100 dpa

Time of computation increases dramatically with dose if only Master equation is used

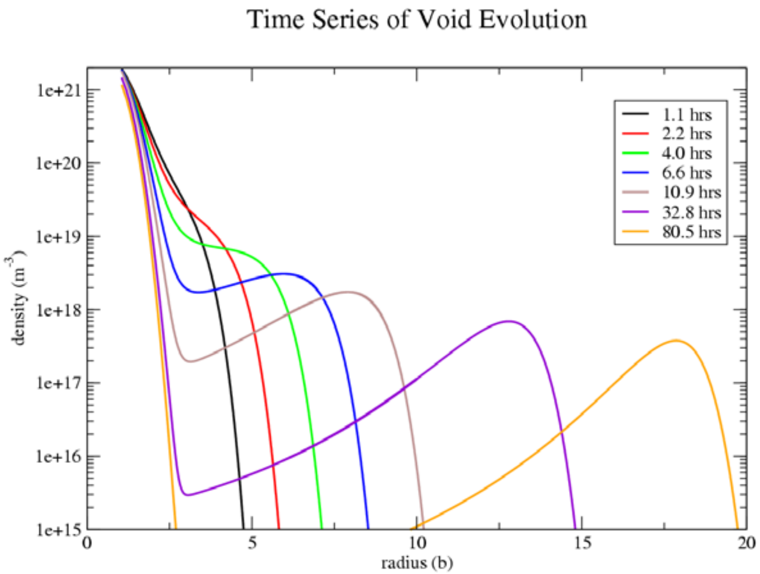

Time of computation is almost linear with dose by combining three methods

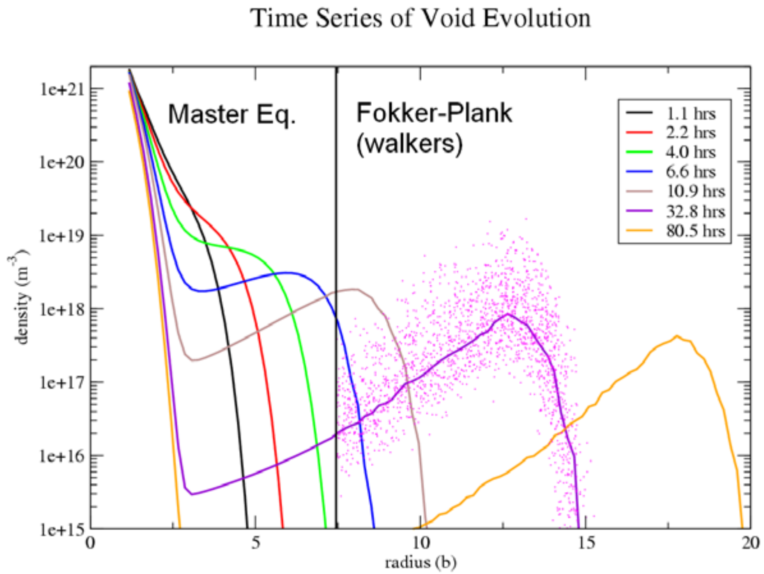

$$\frac{dP(x,t)}{dt} = \beta(x-1)P(x-1,t) + [\alpha(x+1)+\phi(x+1)]P(x+1,t) - [\alpha(x)+\beta(x)+\phi(x)]P(x,t)$$

Void swelling develops in 3 stages: Incubation, Transient, and Steady-State

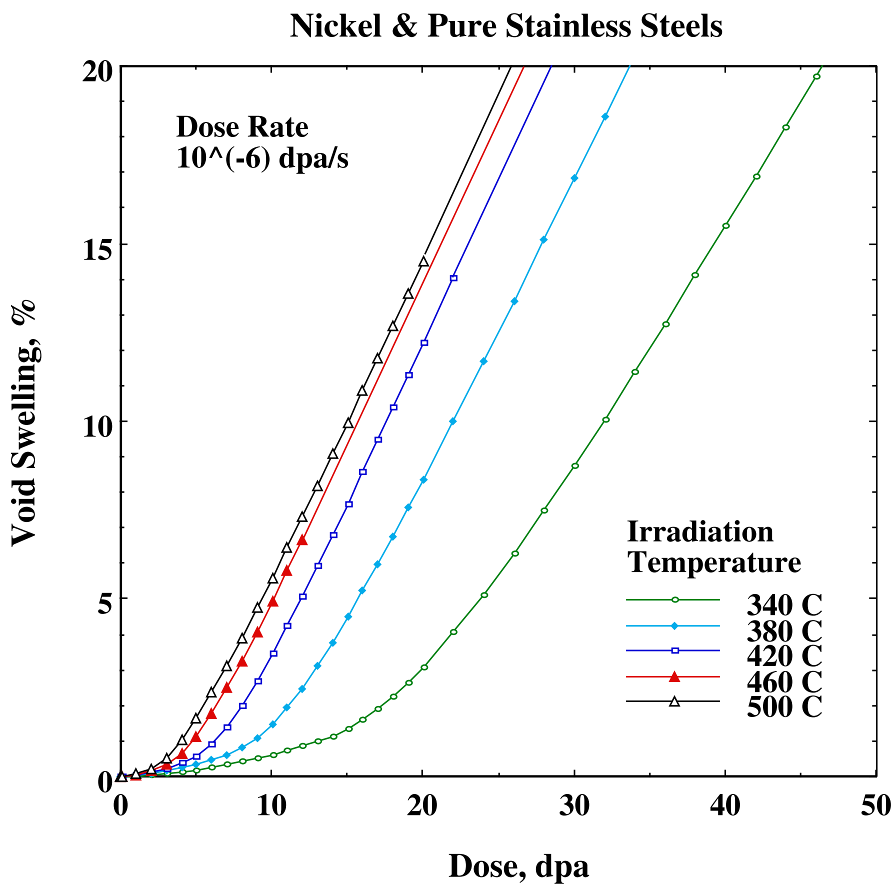

Incubation dose depends on temperature dose rate, dislocation density, etc., but steady-state is nearly independent of all these variables.

A stochastic void nucleation and growth code coupled to dislocation evolution has been developed which reproduces these observed features.

Comparison of swelling rates with two-component rate theory using TEM data

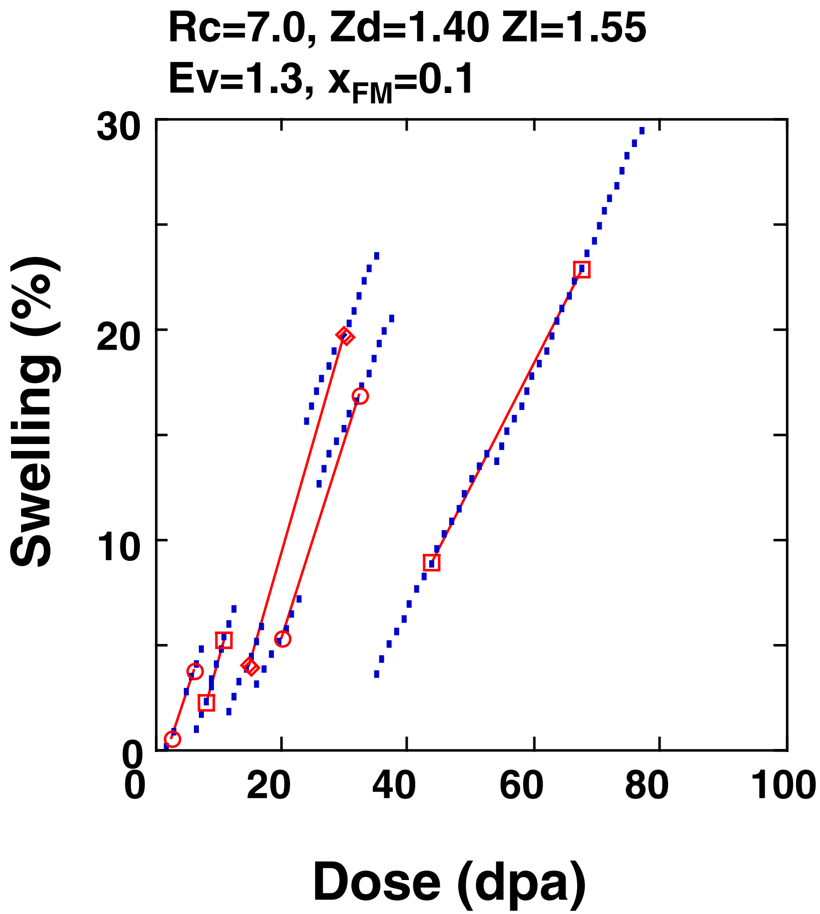

The standard rate-theory works quite well and fitted the parameters are well within the error bars.

rc	bias		Ev	x_{FM}
	Zd	Zl		
3. 5	1.25	1.40	1.4	0.2
3.5	1.40	1.55	1.2	0.1
3.5	1.40	1.55	1.3	0.1
7.0	1.25	1.4	1.3	0.2
7.0	1.40	1.55	1.3	0.1
7.0	1.25	1.4	1.4	0.2

Dotted lines are the predicted swelling trends at the experimentally achieved doses and for the observed defects. Data points are the measured swelling values. Red lines are the empirical swelling trends.

The incubation dose for void swelling depends strongly on the dose rate.

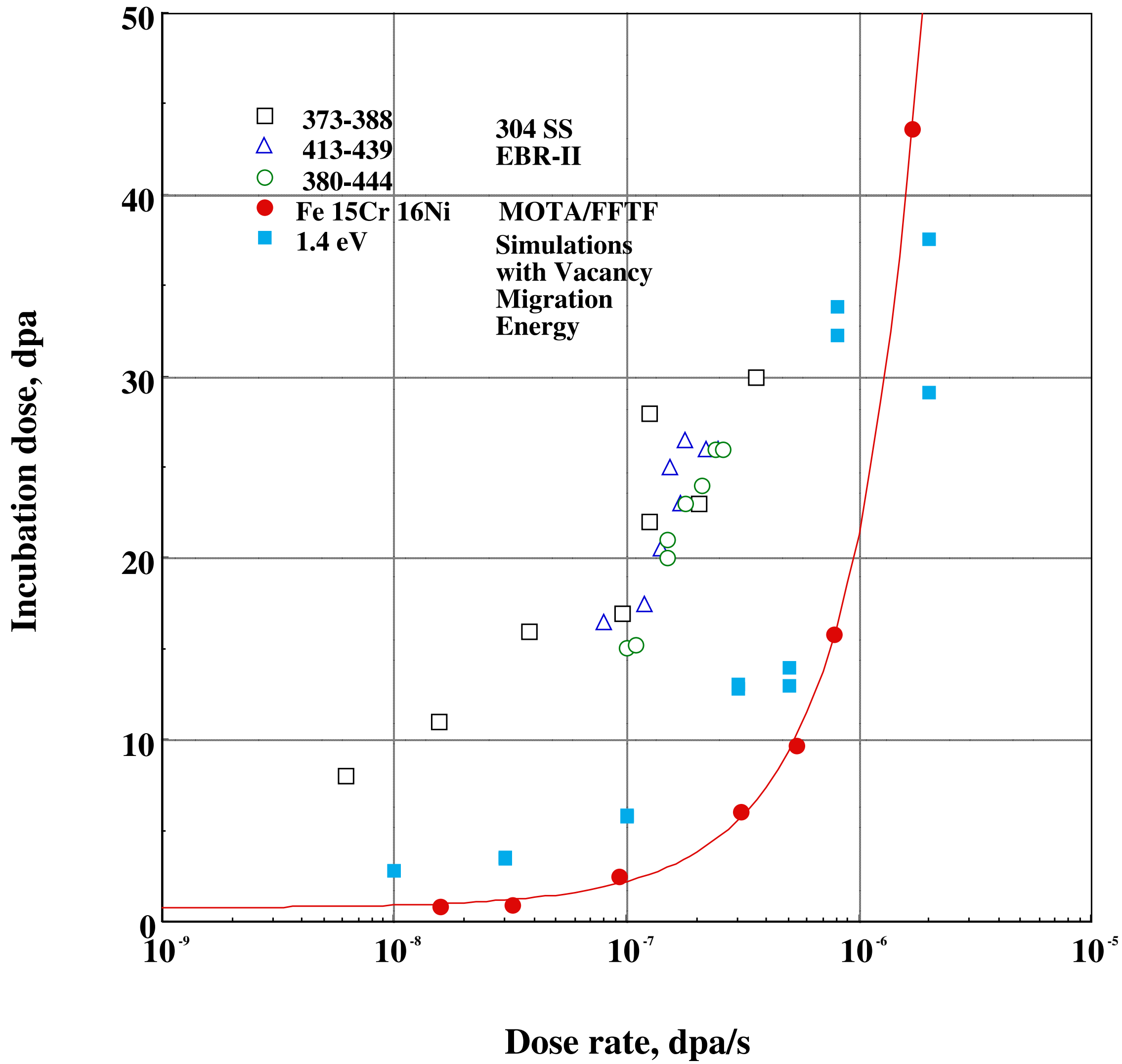

Simulations can reproduce the incubation doses for pure austenitic alloys, but not yet for commercial steels.

Void & Bubble Swelling is also found in LWR's

PNNL

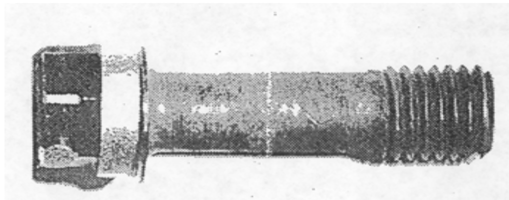

Cavities in Tihange 316 SS Baffle Bolt

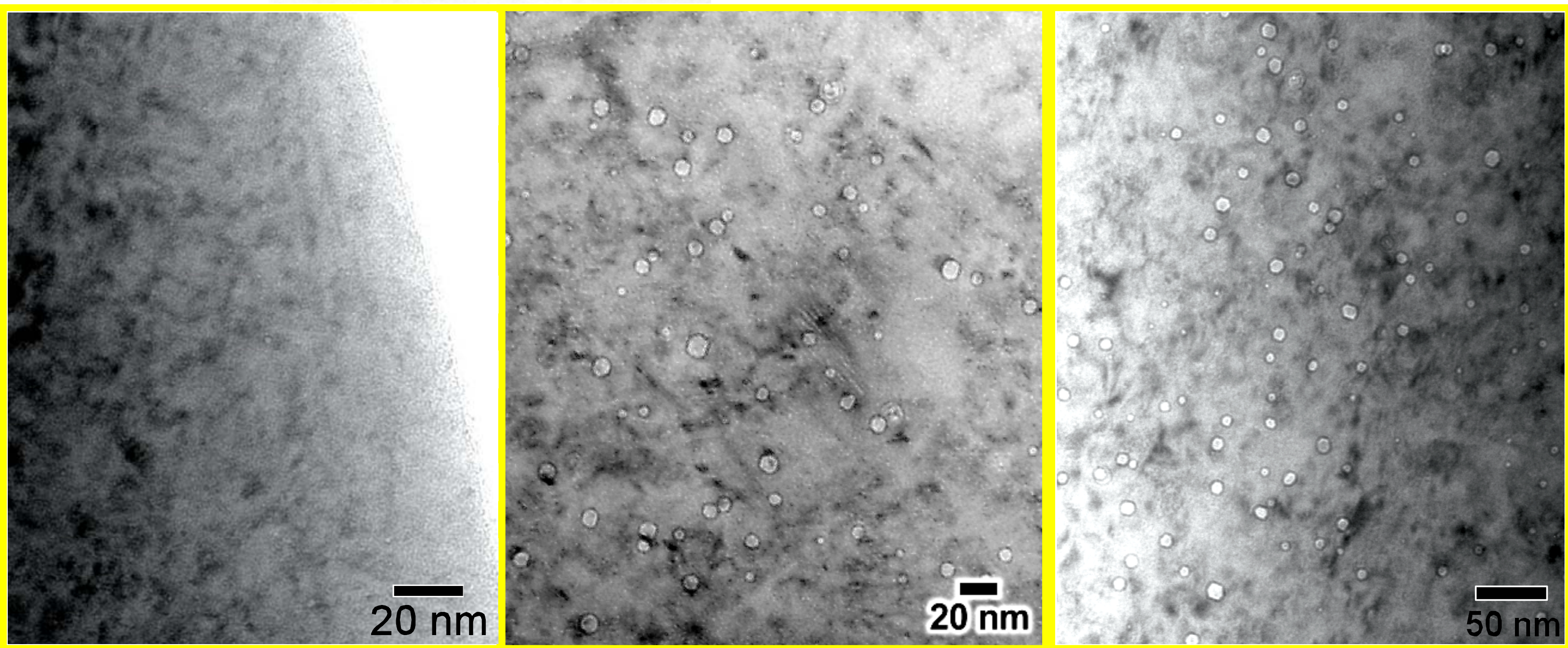

Bolt Head, 0 mm
14 dpa, ~320°C

Top Shank, 25 mm
10 dpa, ~340°C

Near Threads, 57 mm
7 dpa, ~330°C

Simulation results predict a strong effect of dislocation density on the onset of void swelling.

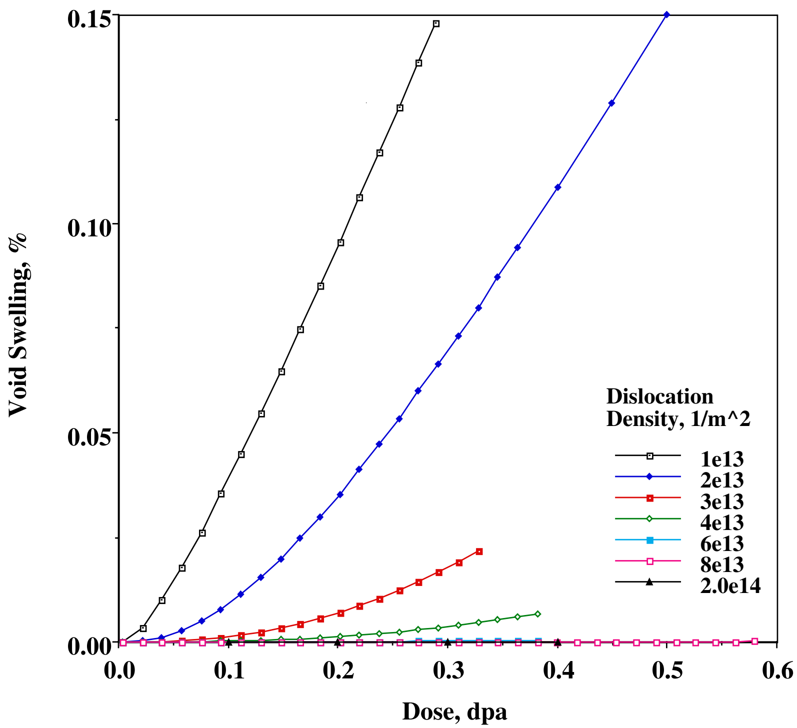

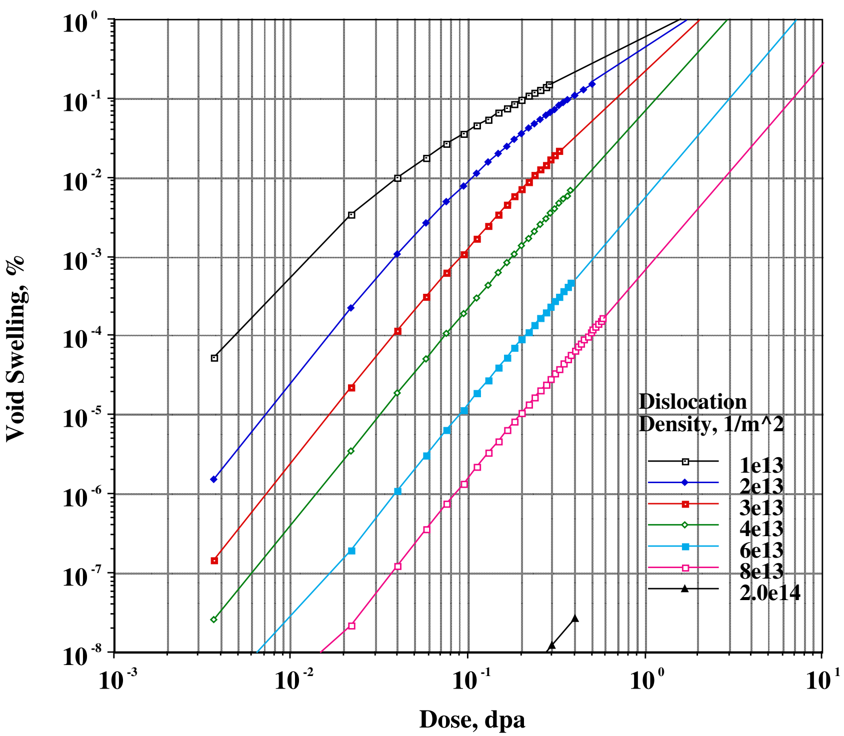

The code predicts <u>for the first time</u> a realistic incubation stage for void swelling followed by a linear stage.

The Dislocation Density evolves during Irradiation

W.G. Wolfer & B.B. Glasgow, Acta Met. 33 (1985) 1997

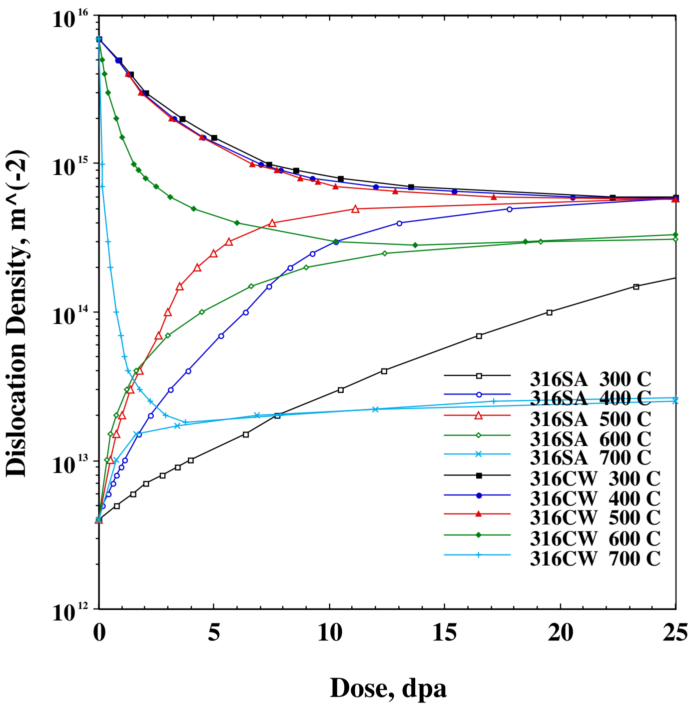

Loop growth and coalescence plus climb of segments increase the density, but climbing and gliding segments of dislocation dipoles lead to annihilation. Eventually, a saturation density may be reached.

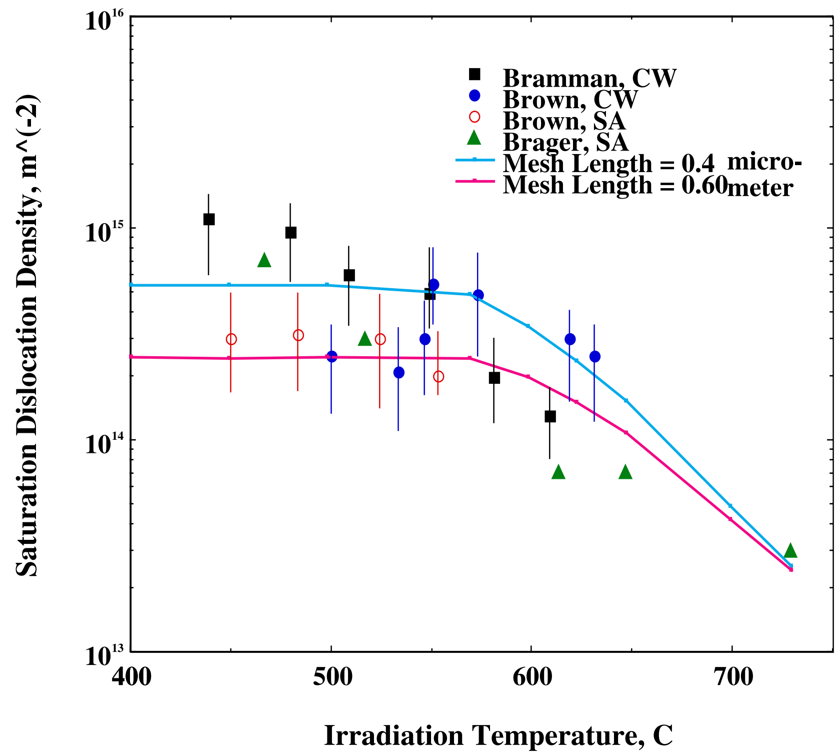

Since evolution begins prior to void formation, dislocation can not all have the same bias.

Loop evolution must be included as a separate sink component.

What determines the mesh length ?

Dose rate affects dislocation loop formation, growth and unfaulting

T. Okita, N. Sekimura, T. Sato, F.A. Garner, & L.R. Greenwood, ICFRM-10

Fe 15Cr 16Ni, SA, 408-444 C

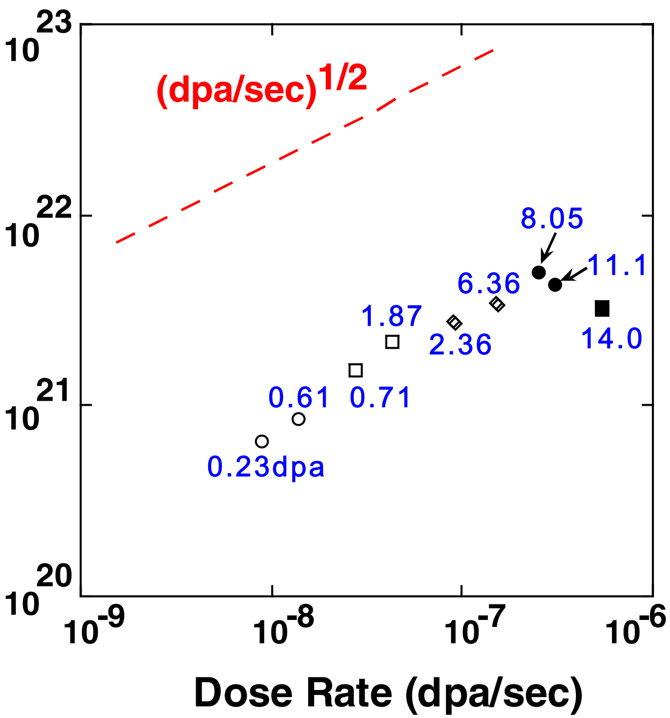

Comparison between the experimental results and model calculation

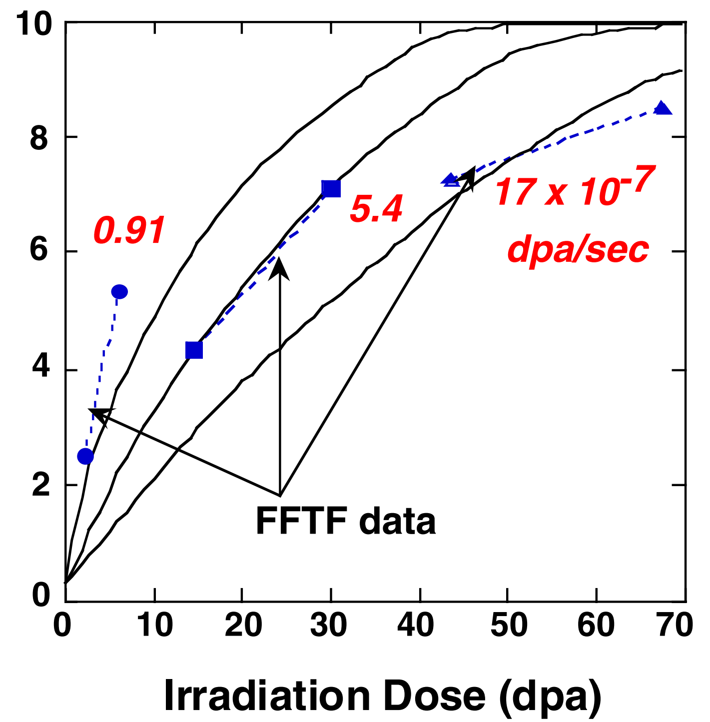

As a result of loop un-faulting and coalescence, the dislocation density also changes faster per unit dose at lower dose rates.

Modeling and simulation the evolution of the dislocation structure remains a major challenge

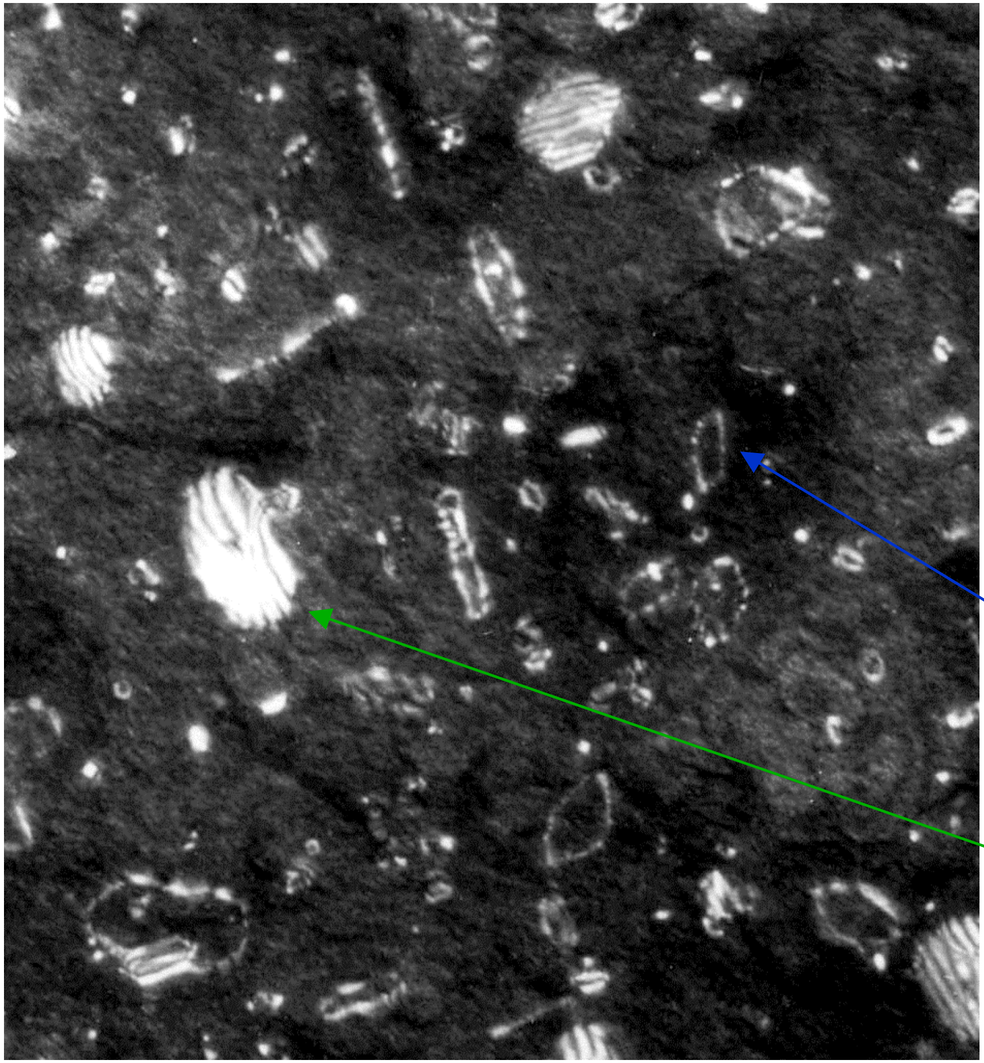

Experimental evidence (Okita, 2003) from ion irradiated steels shows no correlation of unfaulting with loop size, contrary to energy considerations.

Fe-15 Cr-16Ni irradiated with Ni^{3+} at 773 K, 1.0 dpa 4.0×10^{-4} dpa/sec

Perfect loop with the diameter of < 30 nm

Faulted loop with the diameter of > 50 nm

MD Discovers Mechanism for Dislocation Loop Unfaulting

Alison Kubota, Maria-Jose Caturla and Wilhelm Wolfer

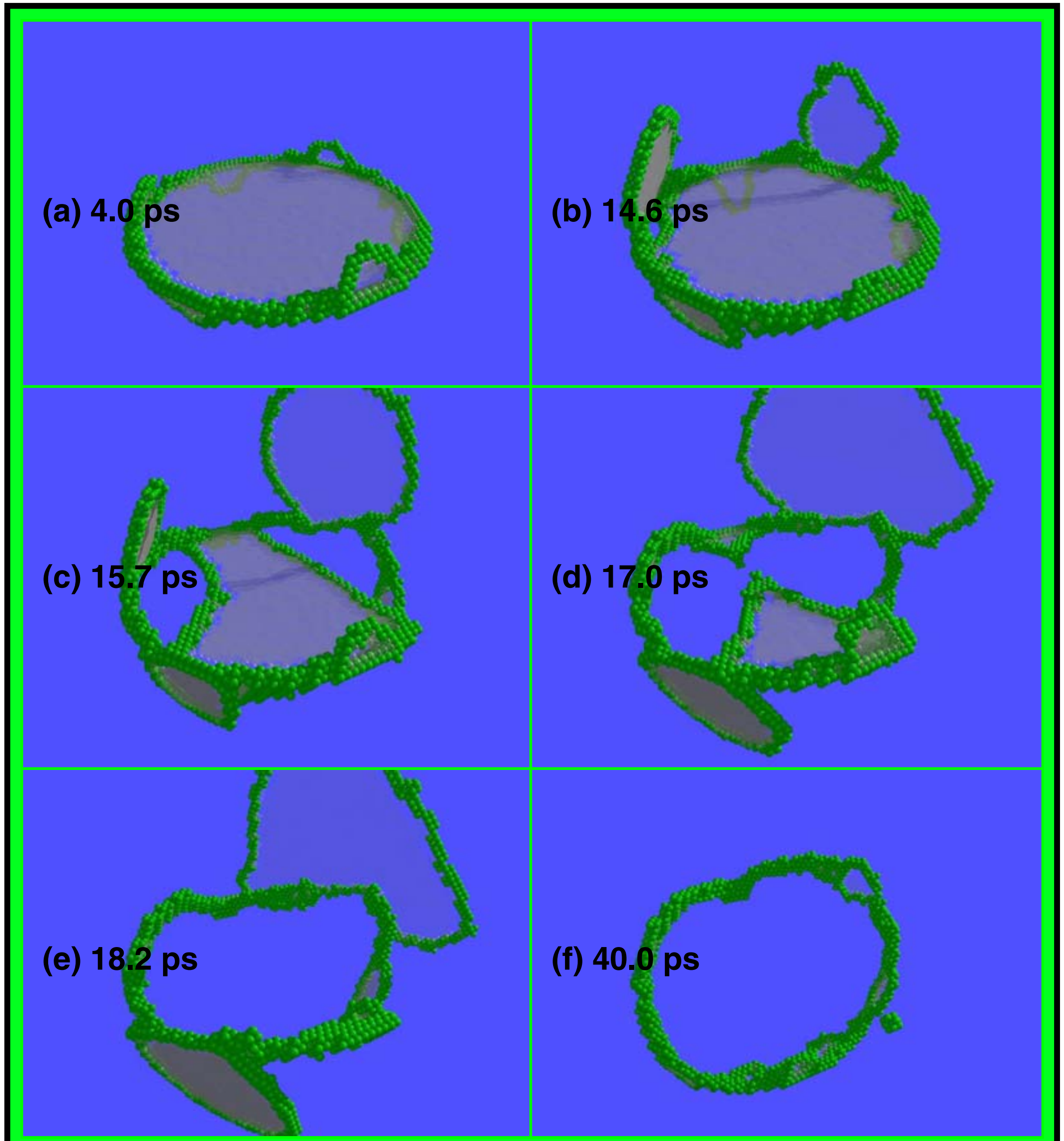

Snapshots of a 4 million atom simulation on 128 MCR CPUs (12 hours) at various stages along a dynamic loop unfaulting pathway. The initial faulted loop (a) undergoes complex dislocation reactions transforming into a glissile perfect loop with a net Burgers vector change (f).

Relevant apects of this work:

- This work uncovers a much deeper and detailed understanding of the phenomena of loop unfaulting in FCC metals. The vast computational capabilities of MCR has enabled the team to systematically probe the parameter space for conditions under which different unfaulting mechanisms can occur.
- This is high profile work with an article in preparation for submission to the journal Science.
- Linear scaling demonstrated beyond 3.5 billion atoms on MCR on this code.
- No MPIAll-to-All or MPIAllReduce operations required.
- Team has demonstrated delivery on the end-product science on MCR and previous science-runs.
- Team has demonstrated capability to make code changes on-the-fly. Inferno variant code was used to help debug the BlueArc filesystems on MCR.

Entirely new processes for growth of secondary defects are discovered by MD

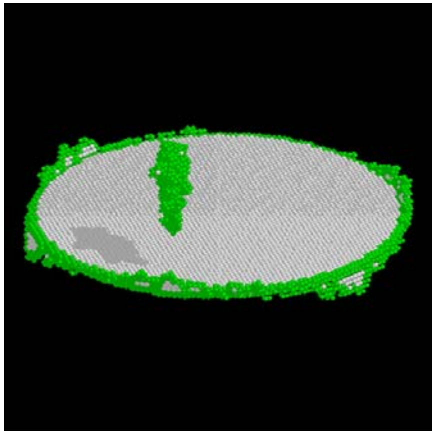

20-keV recoil in 80 x 80 x 80 Ni near fault edge, viewed by CNA.

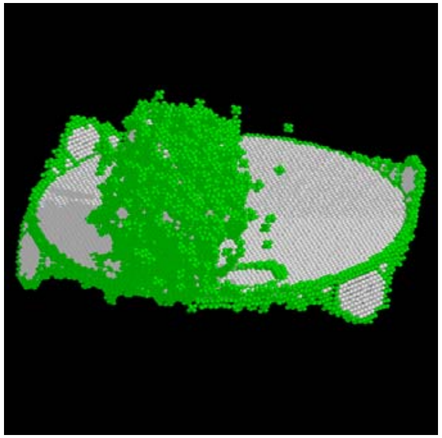

0.65 ps. Dislocation begins to grow on fault surface.

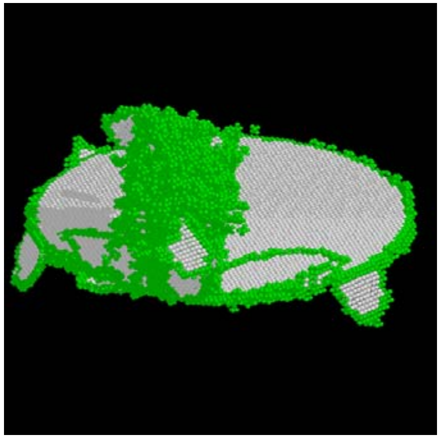

0.91 ps. Maximum growth of surface dislocation. Perfect loop begins to coalesce from cascade debris.

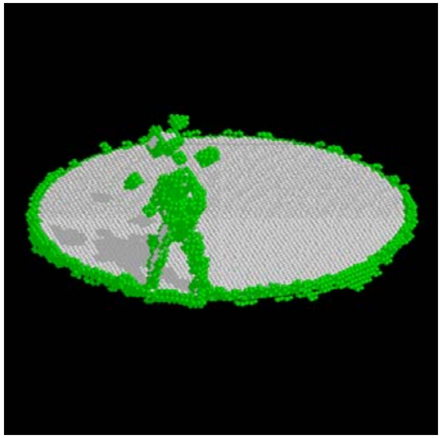

1.65 ps. Surface dislocation retracts. Perfect loop forms

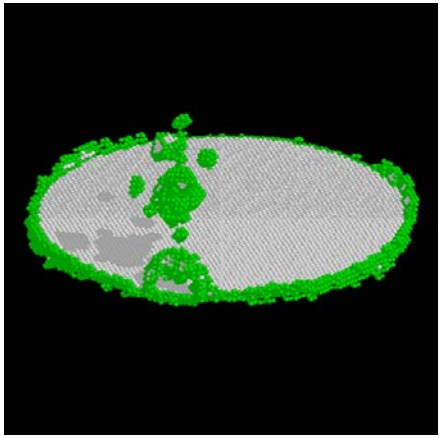

13.15 ps. Perfect loop begins a rapid faulting process.

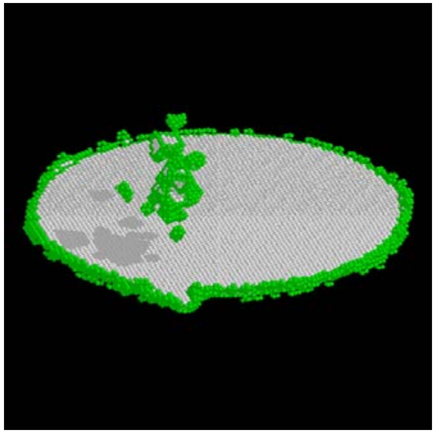

24.15 ps. The interstitial loop from cascade is directly added to the large loop.

Rotation changes the interaction of glissile loops with dislocations

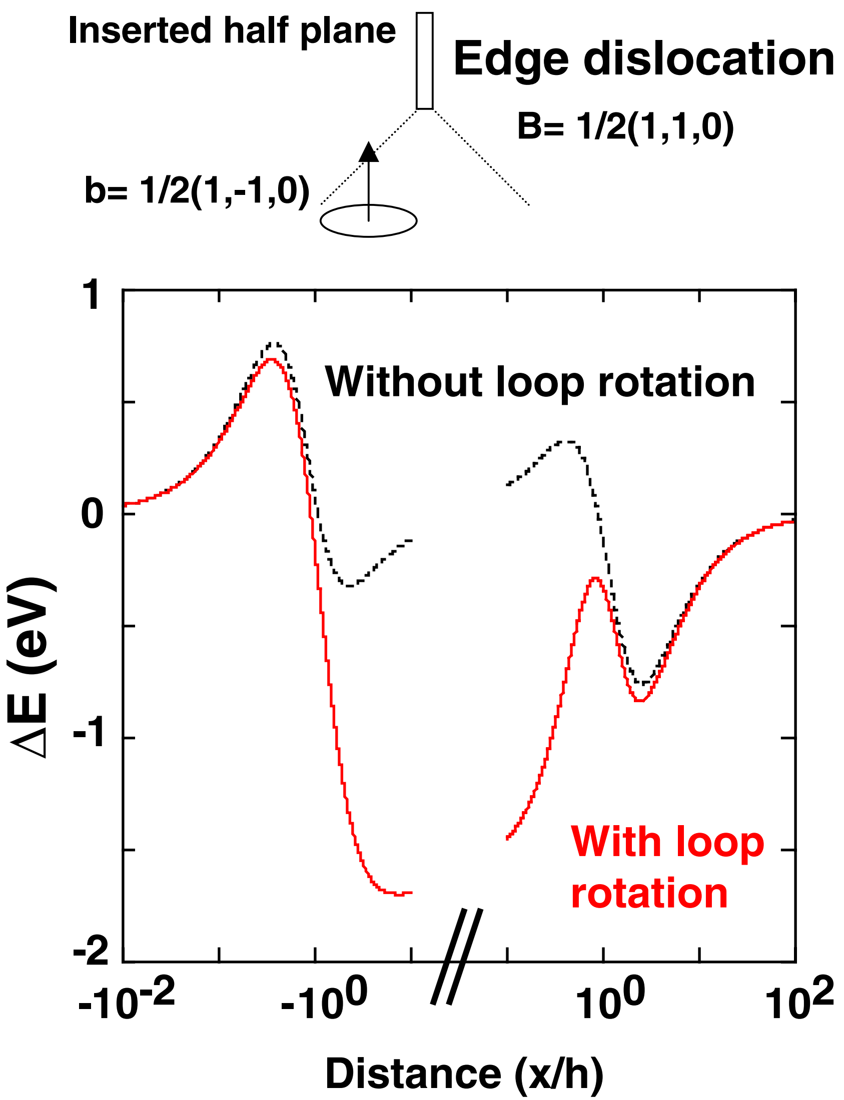

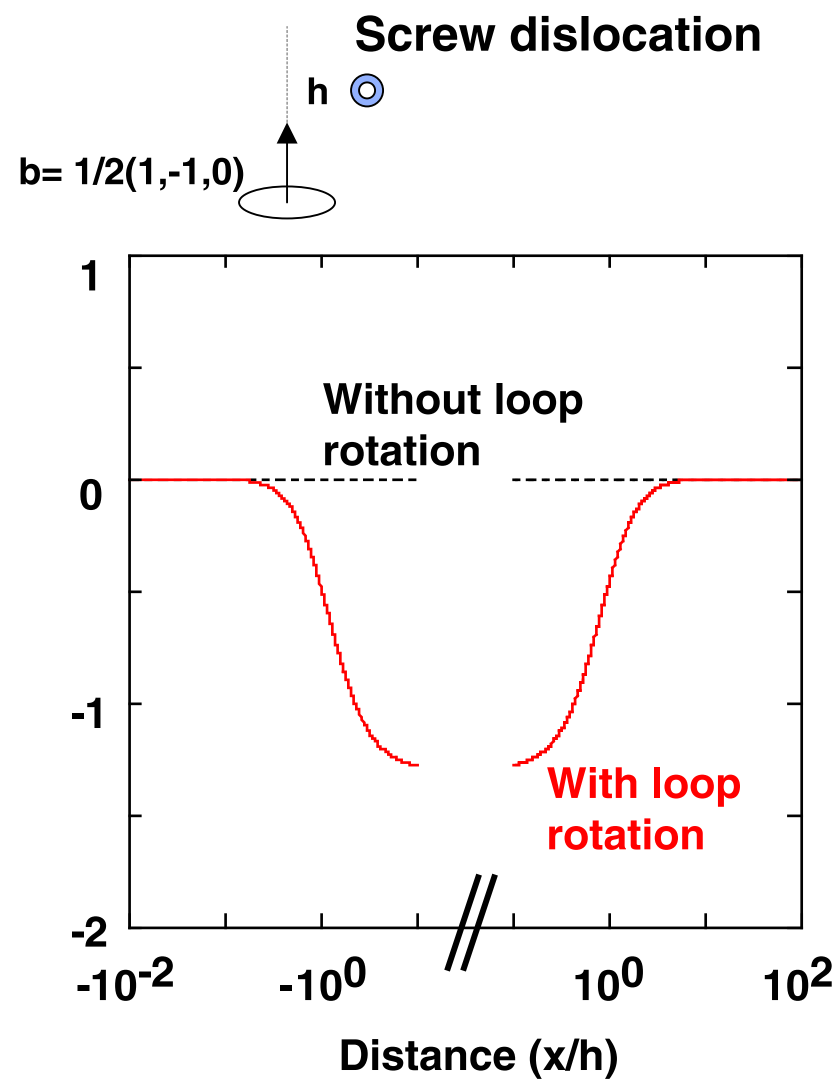

Helium bubbles increase the strength when they are highly over- pressurized

Strengthening models agree well with data on helium bubbles in steels produced by tritium decay. He/V = 2 as inferred from loop punching.

$$\textit{total} \qquad \textit{cut} \qquad P$$

$$\textit{cut} \qquad 0.12\frac{b}{R}\ \ell n\frac{R}{b} \quad 0.644\ S_0$$

$$P \qquad 0.65\left|P \quad \frac{2}{R}\right|^{3/2}\sqrt{GRS_0/b}$$

Advances in simulating complex dislocation configurations and dislocation-defect interactions will greatly improve the predictions

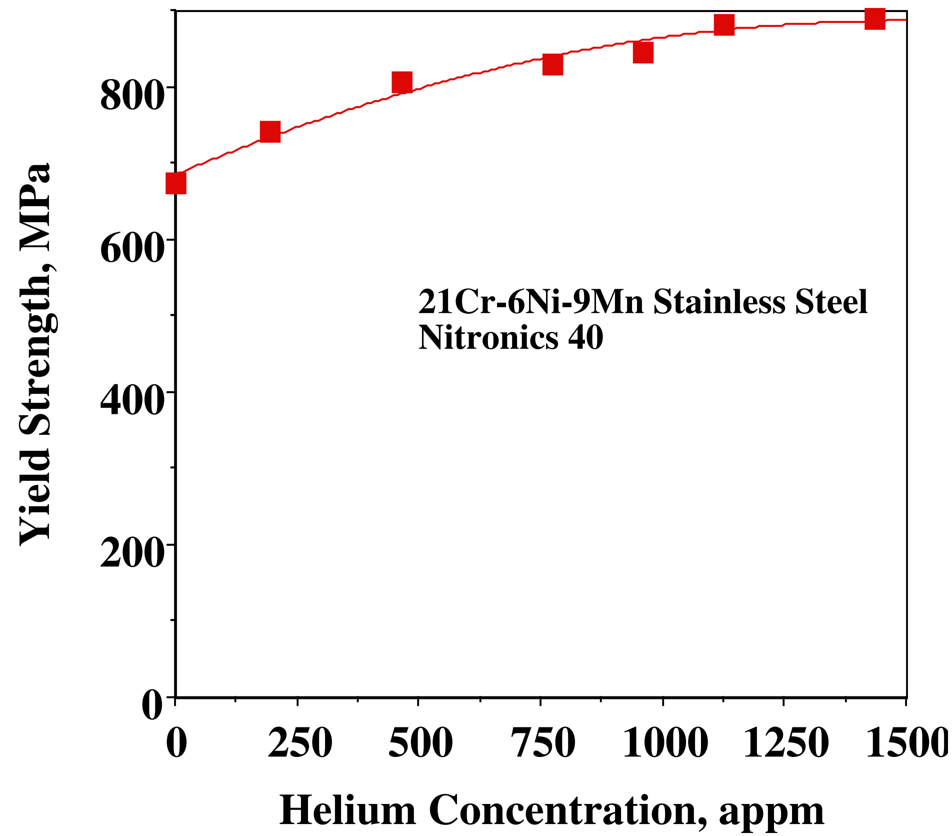

Effective elastic constants can be computed when secondary microstructure is known

Effective compressibility

Compressibility of matrix

Bubble contribution

Effect of compressibility mismatch

Effect of surface tension

$$1$$

$$\frac{1}{K} \quad \frac{1}{K} \qquad \frac{(4G \quad 3K)\,S}{[4G \quad 3K_{He} \quad 4G(1 \quad K_{He}/K)S]} \qquad 1 \quad \frac{K_{He}}{K} \qquad \frac{2(4G \quad 3K)(2 \quad /3rK)}{3K_{He} \quad 4G[1 \quad S(1 \quad K_{He}/K)] \quad (2 \quad /r)[1 \quad 4GS/3K]}$$

Closed-form solutions are possible only for modest swelling S by bubbles,voids, or spherical precipitates.
More complex microstructures can, however, be treated with Finite Element Methods.

Voids in irradiated steels reduce elastic moduli as predicted by theory

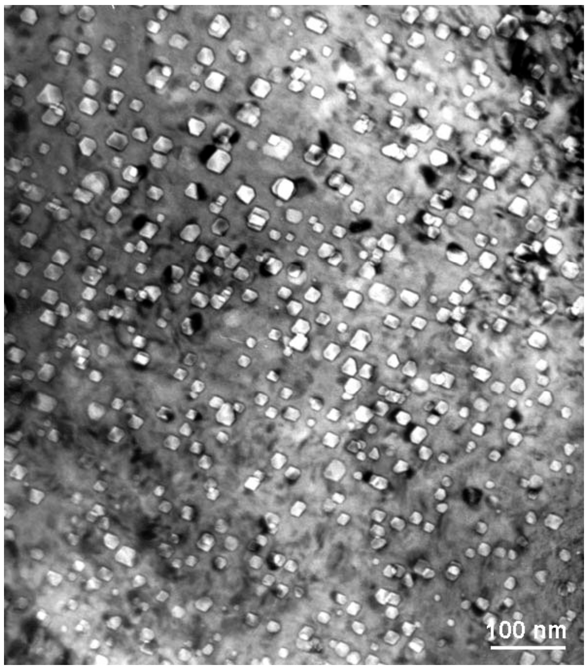

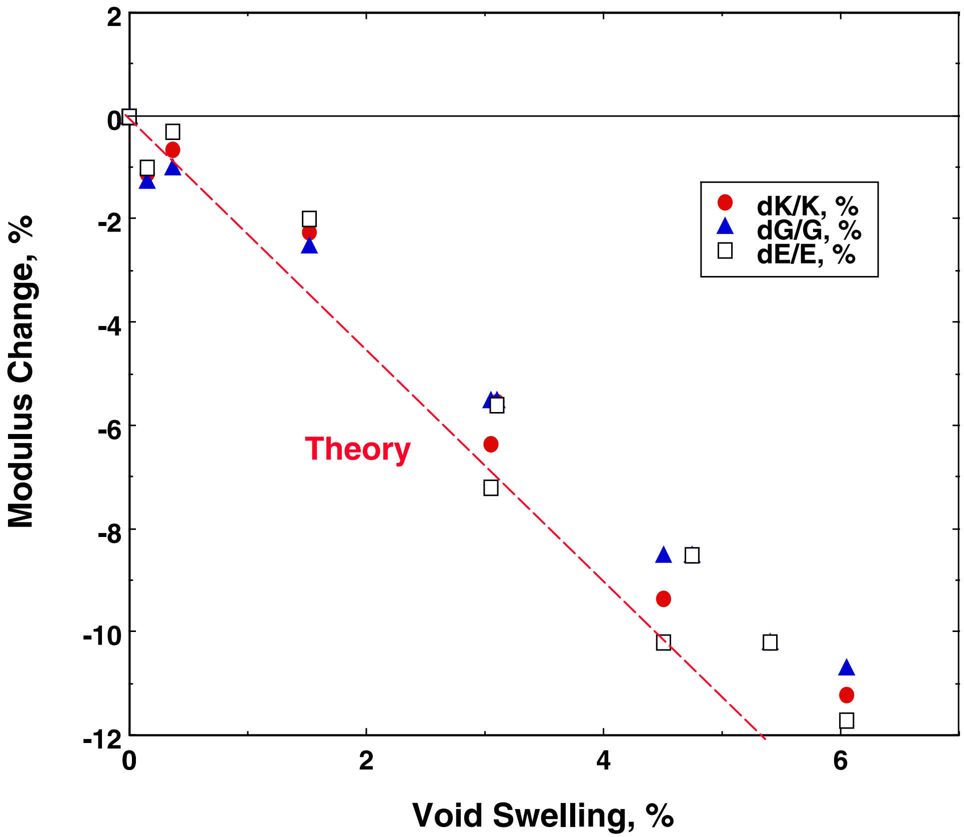

Reference: Kozlov, A.V., Shcherbakov, E.N., Averin, S.A., and Garner, F.A. "**The Effect of Void Swelling on Electrical Resistance and Elastic Modulii in Austenitic Steels**," *Effects of Radiation on Materials: 21st International Symposium, ASTM STP 1447,* M. L. Grossbeck, Ed., ASTM International, West Conshohocken, PA, 2003.

Elements with Void Swelling Observed

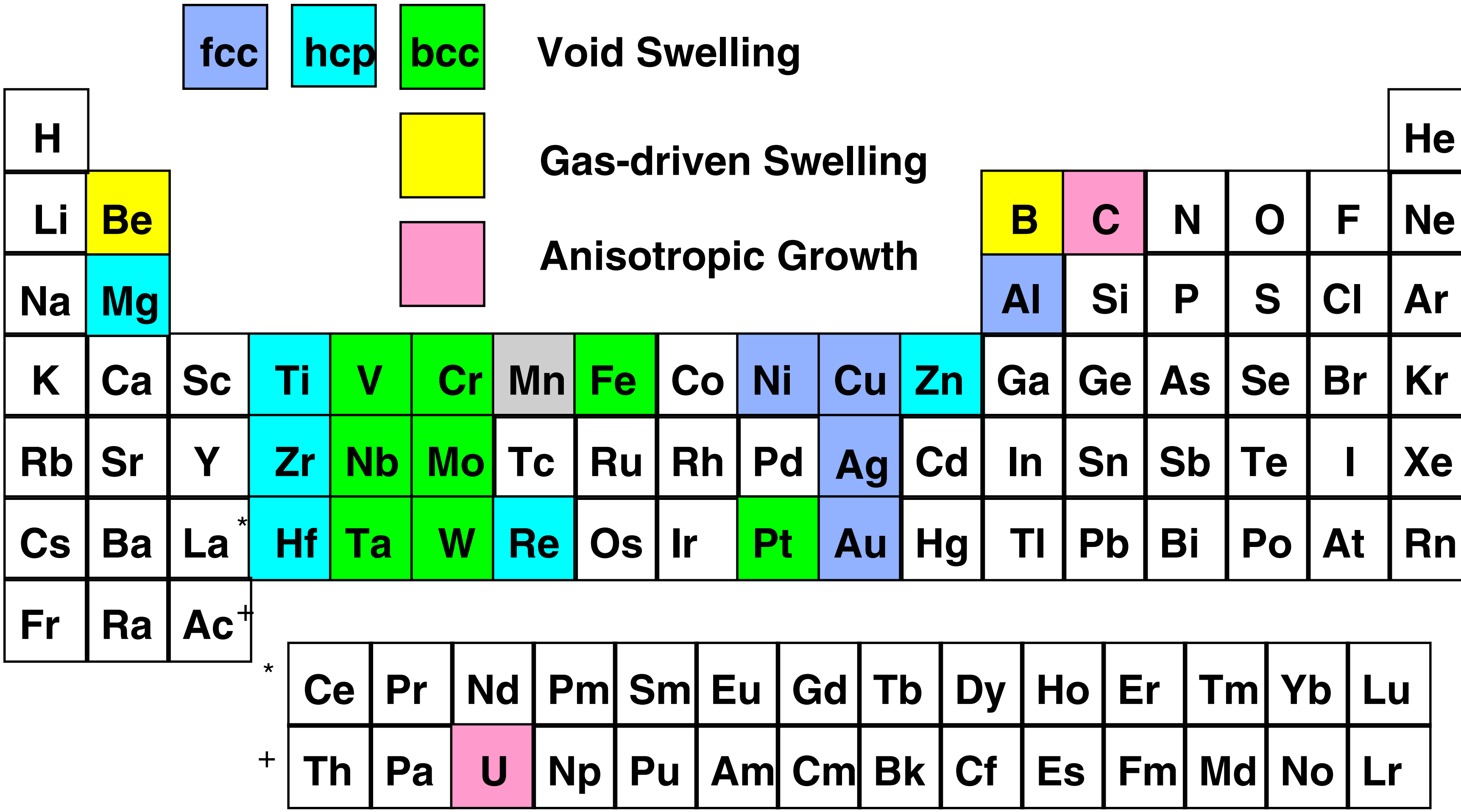

No Element Tested Has Ever Failed to Swell

First-principle calculations are now feasible to predict a material's propensity for void swelling

The Net Bias and propensity for void swelling is governed by Abs(relaxation volume) of interstitial > that of vacancy

The incubation time for void swelling increases 10 fold from Ni to α–Fe, where it is 100 dpa. α–Fe also swells at a rate 5 times lower than Ni.

If our predictions turn out to be correct, δ-Pu should be resistant to void swelling.

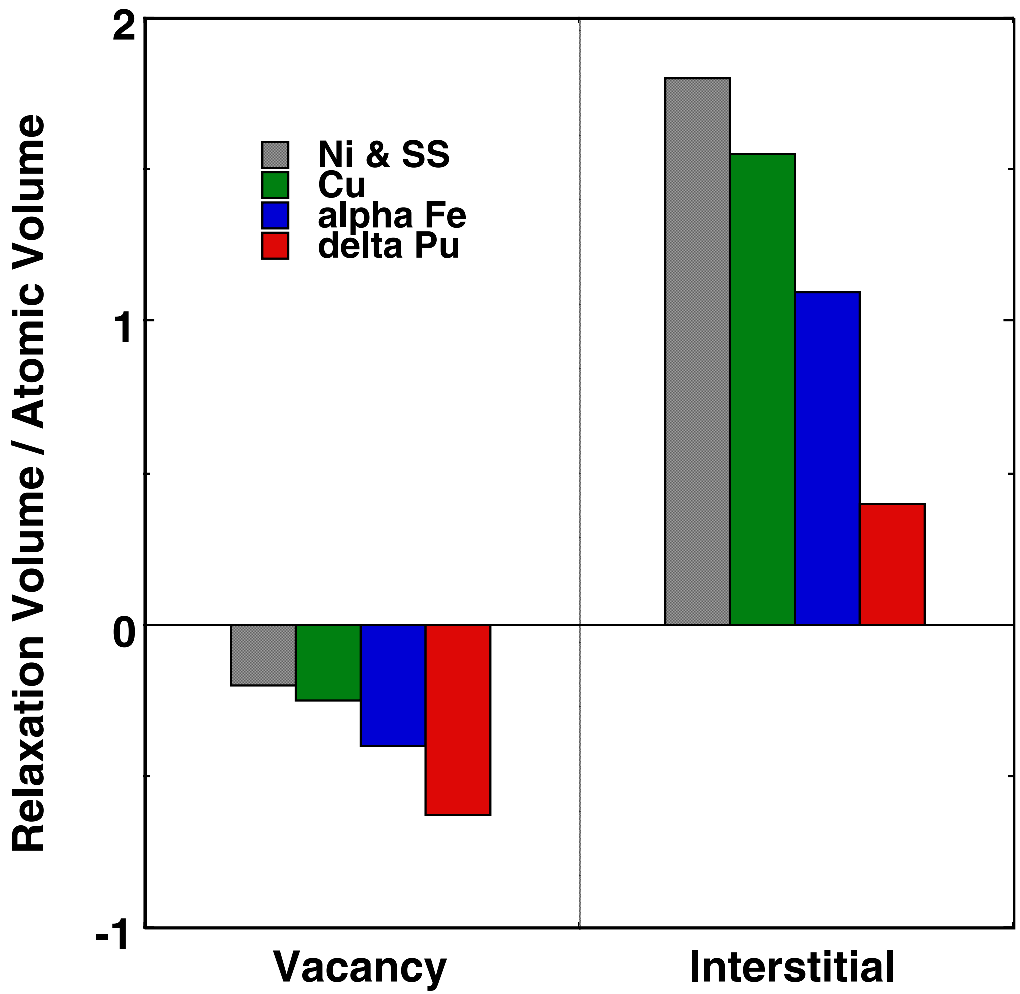

Steady-State Swelling Rates scale with the Net Bias

Contour Lines of constant Net Bias

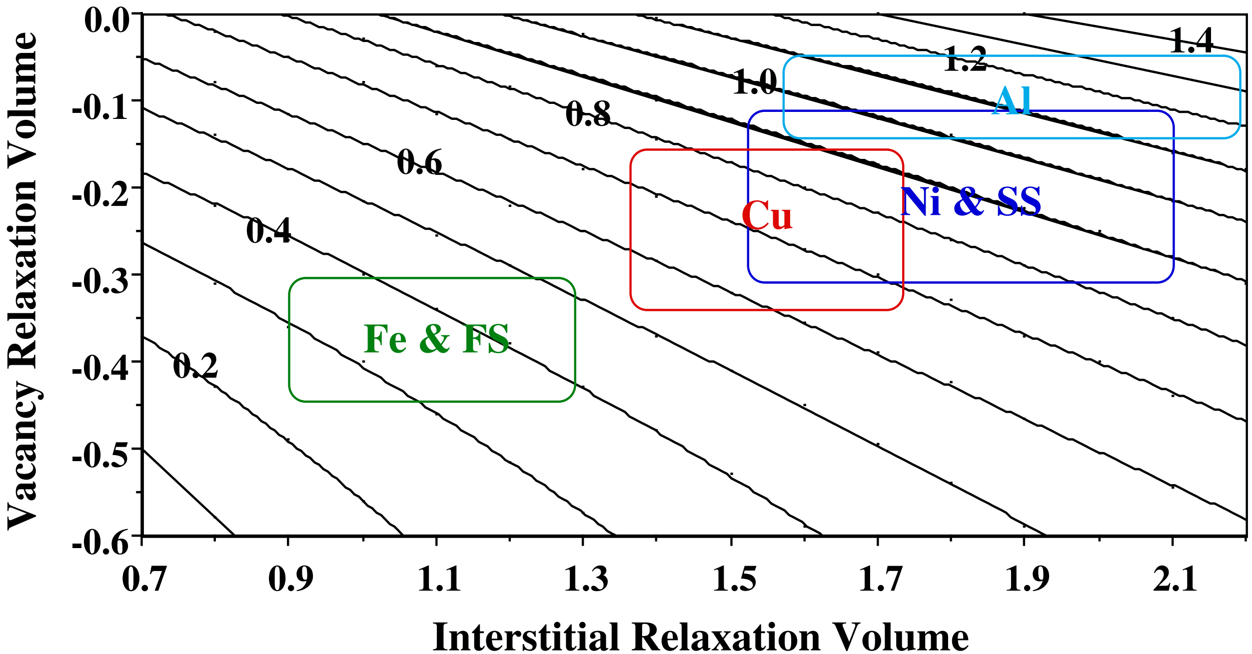

dS/d(dpa) $\leq 12.5\,\xi\,B$ (%/dpa)
Damage Efficiency: $\xi = 0.05 - 0.1$
Net Bias : B (see figure)

Metal	Exp. Rate, %/dpa
Al	1.0
Ni & SS	1.0
Cu	0.5
Fe & FS	0.2

What have we learned, and what must we do for present and future reactors

- Bubbles and voids form naturally in any metal considered as a reactor structural material.
- The process of nucleation and growth is mainly governed by the homologous temperature.
- The greatest influence of temperature, dose rate, alloying elements and impurities is seen in the incubation period for void swelling.
- There is a dramatic difference in incubation for ultra-pure and commercial metals, all in favor of the latter, but we don’t know why.
- Steady-state swelling is governed by the bias and fundamental properties of point defects.
- Properties change with microstructure, and the latter evolves as in a complex system.
- This co-evolution should now be put on a solid scientific base and used to develop materials design correlations which are no longer dependent on their original irradiation sources.